The Nocturnal Boundary Layer: A Case Study Compared with Model Calculations

F. T. M. NIEUWSTADT AND A. G. M. DRIEDONKS

Royal Netherlands Meteorological Institute, De Bilt, The Netherlands

(Manuscript received 9 February 1979, in final form 25 July 1979)

ABSTRACT

A case study of nocturnal boundary-layer development is presented. The data include observations of turbulence and of profiles of wind and temperature. The measurements were done along a 200 m high meteorological mast.

The observations are interpreted in terms of the results of a one-dimensional boundary-layer model. The model is derived from the full set of equations governing the evolution of the nocturnal boundary layer by neglecting advection. The validity of this approximation is discussed.

From a comparison of observations and calculated results it follows that the influence of advection is important especially in the upper part of the boundary layer. Nevertheless, we find that important characteristics of the nocturnal boundary layer such as its height can be reasonably well simulated by a one-dimensional model.

1. Introduction

The boundary layer during a clear night contrasts with the convective boundary layer in the daytime. In the latter, turbulence is produced by buoyancy leading to large turbulent fluxes and to rapid vertical exchange. This means that the convective boundary layer is primarily locally determined. Advection plays a secondary role.

In the nocturnal boundary layer radiational cooling of the surface leads to a stable temperature gradient. Turbulence is then suppressed by negative buoyancy. In a shallow layer near the surface turbulence of small intensity can be maintained by mechanical production. Because vertical exchange in this layer is now small, advection quickly becomes important, as we will discuss in Section 2.

A full solution of the nocturnal boundary layer including advection will lead to a three-dimensional mesoscale model. An adequate description of advection in such a model requires a high horizontal resolution resulting in a large computational effort. However, the results of such a complicated model will still be questionable, primarily because at the moment there are no initial and boundary conditions available of a compatible resolution.

To simulate the nocturnal boundary layer, we have used here a one-dimensional model in which advection is neglected. With such a model vertical profiles are calculated as a function of time. The computation time is negligible compared to that required for the solution of a three-dimensional model. However, the usefulness of this model in which terms known to be important are left out must follow from a direct comparison with observations. This will be one of the major topics of this paper.

Above the boundary layer, where turbulent fluxes are zero, the solution of a one-dimensional model reduces to the well-known inertial oscillation of the wind vector (Blackadar, 1957). Models based on this oscillation (Thorpe and Guymer, 1977) can explain the low-level wind maximum which is frequently observed in the nocturnal boundary layer. For the boundary layer itself, models have been proposed, for example, by Delage (1974), Blackadar (1976) and Brost and Wyngaard (1978). Here we largely follow the approach taken by Delage (1974) as described in Section 3.

For the night of 8–9 February 1975 a fairly complete set of data has been measured along the 200 m high meteorological mast at Cabauw in the Netherlands. Details of the experiments are given in Section 4.

In Sections 5 and 6 these observations are discussed in terms of the characteristics of the nocturnal boundary layer. The measurements are compared with the results of our one-dimensional boundary-layer model. The deviations between observed and calculated results can be attributed to the neglected advection terms; in our case mainly temperature advection. However, we will show that the major features of the nocturnal boundary layer are reasonably well represented by our simple model.

0021-8952/79/111397-09$06.25

2. Equations of motion; the assumption of horizontal homogeneity

If the atmosphere is assumed to be in hydrostatic equilibrium, the continuity and momentum equations for the mean flow in the atmospheric boundary layer (Busch, 1973) are

$$\frac{\partial w}{\partial z} = -\nabla_H \cdot \mathbf{u}_H, \tag{1}$$

$$\frac{\partial \mathbf{u}_H}{\partial t} + \mathbf{u}_H \cdot \nabla_H \mathbf{u}_H + w \frac{\partial \mathbf{u}_H}{\partial z} = -f\boldsymbol{\eta} \times (\mathbf{u}_H - \mathbf{u}_g - \mathbf{u}_{th}) + \frac{\partial}{\partial z} \tau_H/\rho, \tag{2}$$

with $\mathbf{u}_H = (u,v)$, $\nabla_H = (\partial/\partial x, \partial/\partial y)$ and $\boldsymbol{\eta} \times \mathbf{u}_H = (-v,u)$, where $\mathbf{u}_H$ is the horizontal mean wind vector, with components u in the x direction and v in the y direction, w is the vertical velocity component, $\boldsymbol{\eta}$ the unit vector in the vertical direction, f the Coriolis parameter, ρ the air density and τ_H the horizontal Reynolds stress vector (viscous stresses are neglected). The geostrophic wind at ground level $\mathbf{u}_g$ and the thermal wind $\mathbf{u}_{th}$ are defined by

$$\mathbf{u}_g = -\frac{1}{f} \boldsymbol{\eta} \times \frac{1}{\rho} \nabla_H p_0, \tag{3}$$

$$\mathbf{u}_{th} = \frac{g}{fT} \int_0^z \boldsymbol{\eta} \times \nabla_H \theta dz, \tag{4}$$

where p_0 is the pressure at ground level; g is the gravitational acceleration and T the absolute temperature in the boundary layer.

The potential temperature θ is governed by

$$\frac{\partial \theta}{\partial t} + \mathbf{u}_H \cdot \nabla_H \theta + w \frac{\partial \theta}{\partial z} = -\frac{\partial}{\partial z} \frac{H}{\rho c_p}, \tag{5}$$

in which H is the sensible heat flux and c_p the specific heat at constant pressure. Radiative terms have been neglected.

In order to simplify these equations of motion, we will investigate whether the advection terms in (2) and (5) can be neglected in nocturnal boundary layers. A typical nocturnal boundary layer is characterized by a height $h \approx 200$ m, a cooling rate at ground level of $\sim 1°C\ h^{-1}$ and a geostrophic wind of $\sim 10\ m\ s^{-1}$. The geostrophic velocity deficit, defined as $|\mathbf{u}_H - \mathbf{u}_g|$, is taken as $3\ m\ s^{-1}$. These values are comparable with our measurements discussed in Section 6.

If all the terms in Eqs. (2) and (5) are scaled with these values, we find that horizontal advection can only be neglected if $|\nabla_H \mathbf{u}| \ll 3 \times 10^{-5}\ s^{-1}$ and $|\nabla_H \theta| \ll 3 \times 10^{-5}\ °C\ m^{-1}$. In that case the thermal wind can also be neglected. These restrictions on the horizontal gradients are usually not met in reality. Moreover, in regions with strong vertical gradients (e.g., a sharp inversion) even small vertical motions will cause a large contribution to the vertical advection. Therefore, we must conclude that the advection terms in (2) and (5) cannot be neglected at first hand.

This means, strictly speaking, that the complete set of equations (1)–(5) must be solved in order to simulate the nocturnal boundary layer. In such a three-dimensional model the horizontal and vertical grid spacing are interdependent, when advection and vertical diffusion are treated with equal weight (Barr and Kreitzberg, 1975). Summarizing their argument we express the influence of advection and vertical exchange in (2) in the following schematic way:

$$\frac{\partial \mathbf{u}_H}{\partial t} \approx \frac{\mathbf{V}}{t_a} + \frac{\mathbf{V}}{t_d}, \tag{6}$$

where $\mathbf{V}$ is a characteristic velocity, t_a the time scale for advection and t_d the time scale for diffusion. The solution for (5) can be treated in a similar way. The time scales are connected to characteristic length scales, which we take proportional to the horizontal and vertical grid spacing Δx, Δz. A straightforward estimate of the time scale is given by

$$t_a \approx \frac{\Delta x}{|\mathbf{V}|}, \quad t_d \approx \frac{\Delta z^2}{K}, \tag{7}$$

where K is the vertical exchange coefficient to be discussed in the next section. As the height of the nocturnal boundary layer is of the order of 200 m, we take Δz to be 30 m.

Further characteristic values for K and $|\mathbf{V}|$ in this case are $0.5\ m^2\ s^{-1}$ and $10\ m\ s^{-1}$, respectively. This means that t_a and t_d are of the same order of magnitude when Δx is ~ 20 km. When a wider spacing between horizontal grid points is chosen, t_a will increase or, following (6), the vertical diffusion terms will dominate. The solution at each point will then be effectively given by a one-dimensional model, in which advection is neglected.

A full three-dimensional solution of (1)–(5) with a horizontal grid of 20 km quickly becomes impracticable, even for a moderately sized region. Additionally, initial and boundary conditions of a compatible horizontal resolution are not available, so that a complete solution of (1)–(5) is not yet possible. Instead we used a one-dimensional model despite its limitations. A direct comparison with observations, as given in Section 6, will show which characteristics can still be adequately simulated with such a model.

3. Description of the model

Our one-dimensional boundary-layer model is similar to the models developed by Delage (1974),

Bodin (1976) and Yu (1977). A brief description will suffice here.

Under the assumption of horizontal homogeneity (1)–(5) reduce to

$$\frac{\partial \mathbf{u}_H}{\partial t} = -f\boldsymbol{\eta} \times (\mathbf{u}_H - \mathbf{u}_g) + \frac{\partial}{\partial z}\frac{\boldsymbol{\tau}_H}{\rho}, \tag{8}$$

$$\frac{\partial \theta}{\partial t} = -\frac{\partial}{\partial z}\frac{H}{\rho c_p}. \tag{9}$$

The turbulent fluxes are expressed in terms of the gradients by

$$\frac{\boldsymbol{\tau}_H}{\rho} = K_M \frac{\partial \mathbf{u}_H}{\partial z}, \tag{10}$$

$$-\frac{H}{\rho c_p} = K_H \frac{\partial \theta}{\partial z}. \tag{11}$$

The exchange coefficients $K_{M,H}$ have the form (Delage, 1974)

$$K_{M,H} = l_{M,H}(ce)^{1/2}, \tag{12}$$

where $l_{M,H}$ are the length scales for momentum and heat flux respectively, e is the turbulent kinetic energy per unit mass and c a nondimensional constant. We need an additional equation for the kinetic energy; it reads (Delage, 1974)

$$\frac{\partial e}{\partial t} = \frac{\boldsymbol{\tau}_H}{\rho} \cdot \frac{\partial \mathbf{u}_H}{\partial z} + \frac{g}{T}\frac{H}{\rho c_p} + \frac{\partial}{\partial z} K_M \frac{\partial e}{\partial z} - \frac{(c'e)^{3/2}}{l_M}. \tag{13}$$

In the limit as $z \to 0$, Eq. (13) reduces to a balance between mechanical production and dissipation. Consistency between (12) and (13) then leads to the requirement that $c' = c$. Following Yu (1977) and Bodin (1976), we take $c = 0.2$.

The system of equations (8)–(13) is closed by specifying the length scales l_M and l_H. Yu (1977) has examined a number of expressions for the length scales. Both he and Djolov (1974) obtain good results with the formulation

$$l_{M,H}^{-1} = \frac{\Phi_{M,H}(z/L)}{kz} + \frac{f}{\alpha|\mathbf{u}_g|}, \tag{14}$$

where α is a constant taken here as 4×10^{-4} (Delage, 1974). The specification for the dimensionless velocity and temperature gradients Φ_M and Φ_H is adopted from Businger *et al.* (1971). In order to be consistent with their results, the von Kármán constant is taken as 0.35. The gradients in (14) are taken as a function of the local Obukhov length L, which is given by

$$L = -\frac{Tc_p}{kg\rho^{1/2}}\frac{|\boldsymbol{\tau}_H|^{3/2}}{H}. \tag{15}$$

In order to solve (8)–(13) boundary and initial conditions must be specified. The upper boundary conditions are given at an arbitrary height z_J far above the top of the nocturnal boundary layer. They read

$$\left.\begin{aligned} &\mathbf{u}_H = \mathbf{u}_g \\ &\frac{\partial \theta}{\partial z} = 0, \quad \frac{\partial e}{\partial z} = 0 \end{aligned}\right\} \quad \text{for} \quad z = z_J. \tag{16}$$

The conditions at the lowest calculation level z_1 are

$$\left.\begin{aligned} &\mathbf{u}_H = \frac{\boldsymbol{\tau}_H}{k(\rho|\boldsymbol{\tau}_H|)^{1/2}}\ln(z/z_0) \\ &\theta = \theta_0 - 0.74 \\ &\quad \times \frac{H}{k\rho c_p(\rho^{-1}|\boldsymbol{\tau}_H|)^{1/2}}\ln(z/z_0) \\ &\frac{\partial e}{\partial z} = 0 \end{aligned}\right\} \quad \text{for} \quad z = z_1. \tag{17}$$

The first condition relates the stress to the velocity in a way that is consistent with (10), (12) and (14). It states that for small values of z the wind velocity must follow a logarithmic profile and that the velocity is parallel to the stress. The external parameter z_0 in this equation is the roughness length. The second condition states that the temperature must follow a logarithmic law for small values of z consistent with (11), (12) and (14). The temperature θ_0 at roughness height must be specified to describe the surface cooling. It may follow from measurements or it must result from a model in which the radiation processes near the earth's surface are treated. Here the former approach is used.

To obtain initial profiles for all variables we use the following procedure. Taking a neutral temperature profile, which is usually found at the beginning of the night, we run the model without changing external parameters and without temperature forcing until a nearly steady state is reached (small inertial oscillations in the solution remain present). This solution is then used as the initial condition. In this way a stable method of starting the calculations is obtained. However, the actual conditions at the beginning of the night might be far from stationary. This means that errors will be introduced due to the choice of initial conditions. In Section 6 we will discuss these errors; we will show there that they might have a considerable influence on the solution at a later stage, especially at higher levels.

A solution to this system of equations is sought by applying Newton's method. The resulting linear set of equations is solved on a nonuniform grid $z_j, j = 1, \ldots, J$, by the box scheme. This is an implicit difference method particularly suited for parabolic equations (Keller, 1971). The grid size varies

TABLE 1. Continuously measured wind and temperature data at the 213 m mast at Cabauw, the Netherlands, for February 1975.

Element	Instrument	Height (m)	Sampling time (s)	Recording device
Wind speed	Cup anemometers	2, 10, 20, 40 80, 120, 160, 200	120	Paper tape
Wind direction	Wind vane	10, 80, 200	120	Paper tape
Temperature	Ventilated thermocouples	2, 10, 20, 40 80, 120, 160, 200	120	Paper tape
Boundary-layer height	Acoustic sounder	0–1000		Facsimile recorder

from 3 m near the surface to 400 m near the upper boundary. The time step is taken as 360 s.

4. Experimental data

The experimental data were obtained at the 200 m high meteorological mast at Cabauw in the Netherlands (Driedonks *et al.*, 1978).

The profile measurements comprise the wind speed, wind direction and temperature (Table 1). Measurements of turbulence were carried out simultaneously at three levels: 20, 80 and 200 m. Wind fluctuations were measured by a trivane (Wieringa, 1967) and temperature fluctuations by fast-response thermocouples (Driedonks *et al.*, 1978). The sampling frequency was 1 Hz. From these data the turbulent momentum and heat fluxes (averaged over 30 min) were obtained after removal of a linear trend in the data. The height of the turbulent boundary layer was monitored with the help of an acoustic sounder (sodar).

For the measuring period the geostrophic wind was calculated from the pressure data at 19 meteorological stations in the Netherlands by a method based on principal component analysis of a time series of pressure data measured at these stations (Cats, 1977).

Measurements were performed during the night of 8–9 February 1975. Table 2 gives a summary of the data obtained during that night.

The synoptic situation showed a stationary high-pressure area over central Europe leading at the experimental site to a prevailing southeasterly wind of $\sim 10\ \mathrm{m\ s^{-1}}$.

From the synoptic pressure distribution an estimate can be found for the vertical velocity w_h at the top of the boundary layer. First, we apply the operator $\nabla_H \times$ to both sides of (8). Then, after using (10) and the continuity equation (1), the equation for w_h becomes

$$w_h = \frac{K_M}{f}\left(\frac{\partial \zeta}{\partial z}\right)_{z=0}, \tag{18}$$

where $\zeta = \partial v_H/\partial x - \partial u_H/\partial y$ is the vertical component of the vorticity. In the derivation of (18) we assume that ζ is stationary, consistent with the meteorological situation. The $(\partial\zeta/\partial z)_{z=0}$ is estimated as ζ_h/h, where ζ_h is the vorticity at the top of the boundary and h the boundary-layer height. In our case the boundary layer height is 200 m (see Section 6), which is approximately the height of the 1000 mb plane. The ζ_h is calculated with the quasi-geostrophic approximation, which reads (Haltiner, 1971)

$$\zeta_h = \frac{g}{f}\nabla^2 z_h, \tag{19}$$

where z_h is the height of the 1000 mb plane and ∇^2 the Laplace operator. From the weather maps we estimate $\zeta_h \approx 3 \times 10^{-5}\ \mathrm{s^{-1}}$. With a characteristic value of $K_M \approx 0.5\ \mathrm{m^2\ s^{-1}}$ we then find $w_h \approx 10^{-3}\ \mathrm{m\ s^{-1}}$. Considering the error bounds of our estimation procedure this value does not differ significantly from zero. Therefore we will neglect the influence of the vertical velocity.

5. Consistency of closure assumptions

Since measurements of turbulent fluxes and mean profiles are available we can verify the consistency of the closure assumptions in our model. By substituting the observed values of τ_H, H, e, $\partial \mathbf{u}_H/\partial z$ and $\partial\theta/\partial z$ into (10), (11) and (12), we can determine the observed values for the length scales $l_{M,H}$. These must be compared with the result of (14). A comparison for l_M at 80 m is shown in Fig. 1. The results found at the 20 m measuring level are similar (200 m is excluded, because turbulent fluxes were practically zero there). A similar agreement between observed and calculated values is found for l_H. From these results we concude that the flux-gradient relationships (10), (11), (12) and (14) are consistent with our observations.

It is also useful to check for consistency in the value of the constant c in (12). As $c = \tau_H/(\rho e)$ for $z \to 0$ (Delage, 1974), we evaluate its value from our turbulence measurements at 20 m. An average

TABLE 2. Data set for the night of 8–9 February 1975 (times in GMT, which is one hour earlier than LT).

Data set	Time period
30 min averaged mean profiles and acoustic sounder recorder	1430–0300
30 min averaged turbulence statistics and correlations	1830–0330
geostrophic wind	1400–0300

value of 0.18 is found. This agrees well with the value 0.2 used in our model (Section 3).

6. Results and discussion

In our observations the cooling of the air near the surface started at 1430 GMT (1530 LT). We take this as the beginning of the night. Sunset occurred at 1630 GMT.

The calculations were started at 1430 GMT. The temperature profile along the mast was neutral at that time. The initial conditions were determined following the method described in Section 3. We obtained the surface temperature θ_0, which is an external parameter in (17), from a logarithmic extrapolation of the measured temperatures at 9 and 2 m. The roughness length z_0 was taken as 0.2 m (van Ulden *et al.*, 1976).

Fig. 2 shows the observed and calculated heights of the nocturnal boundary layer. We define the boundary-layer height in the model calculations as the height where the turbulent heat flux has decreased to 10% of its value at ground level. It is not clear whether the height where heat flux vanishes is completely equivalent to the boundary-layer height found from the acoustic sounding registration. This equivalence has been discussed for the daytime boundary layer by Frisch and Clifford (1974). However, the agreement between the observed and calculated values is reasonable.

In Fig. 2 we also give the height where the calculated stress decreases to 10% of its value at ground level. Brost and Wyngaard (1978) define the boundary-layer height in this way. This height also approaches a stationary value comparable to the observed results.

Several simple parametric expressions for the stationary boundary-layer height were reviewed by Yu (1978). The most important is a similarity relation

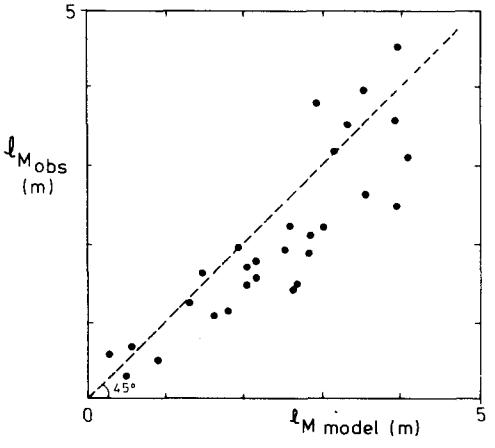

FIG. 1. The comparison between the observed l_M and the l_M following from Eq. (14) for a height of 80 m.

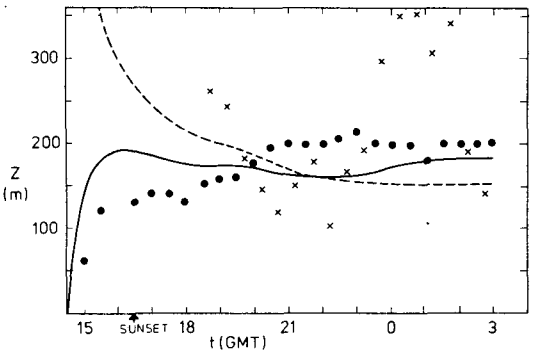

FIG. 2. The height of the nocturnal boundary layer as a function of time: (circles) observed boundary layer height; (crosses) the height given by Eq. (20); (solid line) the height where the calculated heat flux decreases to 10% of its surface value; (dashed line) the height where the calculated stress decreases to 10% of its surface value.

proposed by Zilitinkevich (1975) and by Businger and Arya (1974). It reads

$$h^2 = 0.16 \frac{L}{f} (\rho^{-1} |\tau_H|)^{1/2}, \qquad (20)$$

where both τ_H and L are evaluated in the surface layer ($z \to 0$). The constant 0.16 has been proposed by Brost and Wyngaard (1978). The results calculated with (20) are shown in Fig. 2. In this case (20) poorly predicts the nocturnal boundary-layer height.

In Fig. 3 the calculated and observed potential temperatures at different levels are given as functions of time. The measured and calculated temperatures agree very well at 2 and 9 m. This is not surprising, because the forcing temperature θ_0 in the model is obtained from the measured values at these levels. Here the temperature decreases almost linearly till about 2200 GMT and remains approximately constant after that time. This behavior seems to be inconsistent with the stationary boundary-layer height found in Fig. 2, because according to Brost and Wyngaard (1978) the boundary-layer height can only be truly stationary if there is a persistent constant cooling rate.

Temperature changes due to longwave radiation have been calculated following the method given by Elzasser and Culbertson (1960). They are given for some height intervals in Table 3. These results are based on the temperature and humidity profiles measured along the mast, and on the data of the closest radiosonde launching. They show that the temperature change due to radiation is small inside the boundary layer.

Therefore the differences between model results and observations are caused primarily by neglecting the effects of advection, which were discussed in Section 2. The influence of advection increases

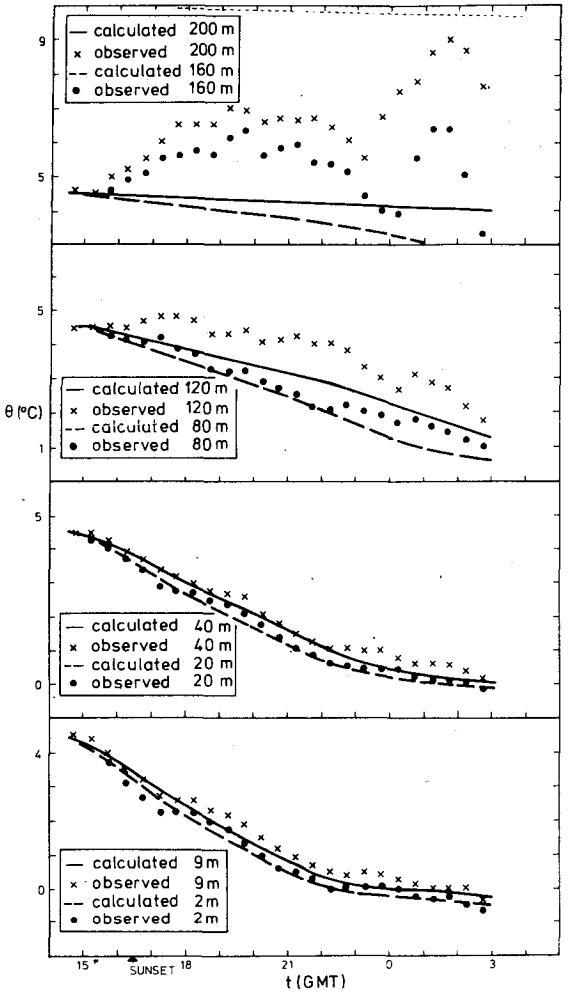

FIG. 3. Measured and calculated potential temperature as a function of time for six observation heights.

with height, because the turbulent fluxes and therefore the vertical exchange decreases with height (Barr and Kreitzberg, 1975). This effect is clearly visible in Fig. 3.

At 200 m the measurements show an average increase of 0.3°C h^{-1}. Since this level is above the boundary layer, the temperature change can only be caused by advection. The horizontal advection can be estimated as follows. In the afternoon the potential temperature is uniform with height over a mixed layer of considerable depth. Therefore, horizontal gradients in this layer can be obtained from surface data. In our case the horizontal gradient was calculated from the surface meteorological observations at 1500 GMT to be 1×10^{-5} °C m^{-1} with a southeasterly direction. As the influence of surface cooling during the night remains confined to the boundary layer which is less than 200 m, we assume that this horizontal gradient does persist above the nocturnal boundary layer. With a measured southeasterly wind of ~10 m s^{-1} this results in an advective temperature change of ~0.3°C h^{-1}, in agreement with the mean temperature change at 200 m.

TABLE 3. Temperature changes due to longwave radiation at 0000 GMT.

Height interval Δh (m)	Temperature change $\partial\theta/\partial t$ in Δh (°C s^{-1})
0–20	2.5×10^{-7}
20–80	1.1×10^{-5}
80–200	2.6×10^{-5}
200–500	-2.6×10^{-5}

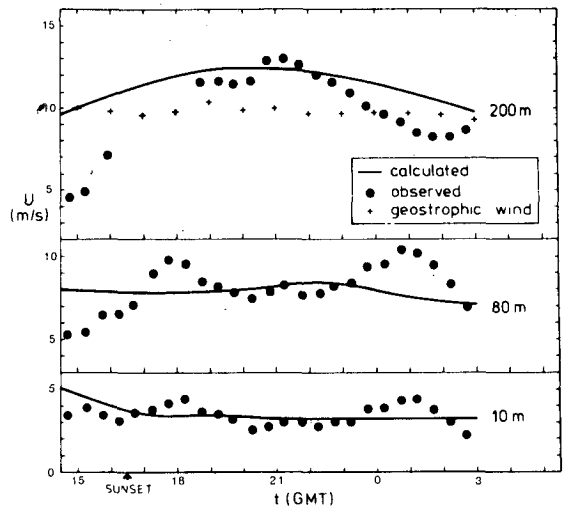

FIG. 4. Measured and calculated wind speed as a function of time for three observation heights.

The wind speed as a function of time is shown in Fig. 4. The initial conditions for the model do not

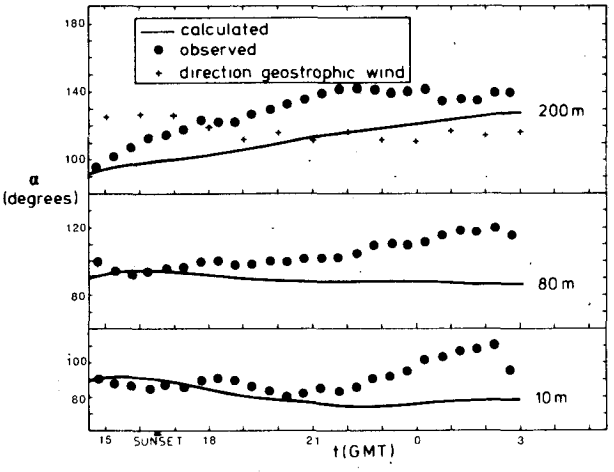

FIG. 5. Measured and calculated wind direction as a function of time for three observation heights.

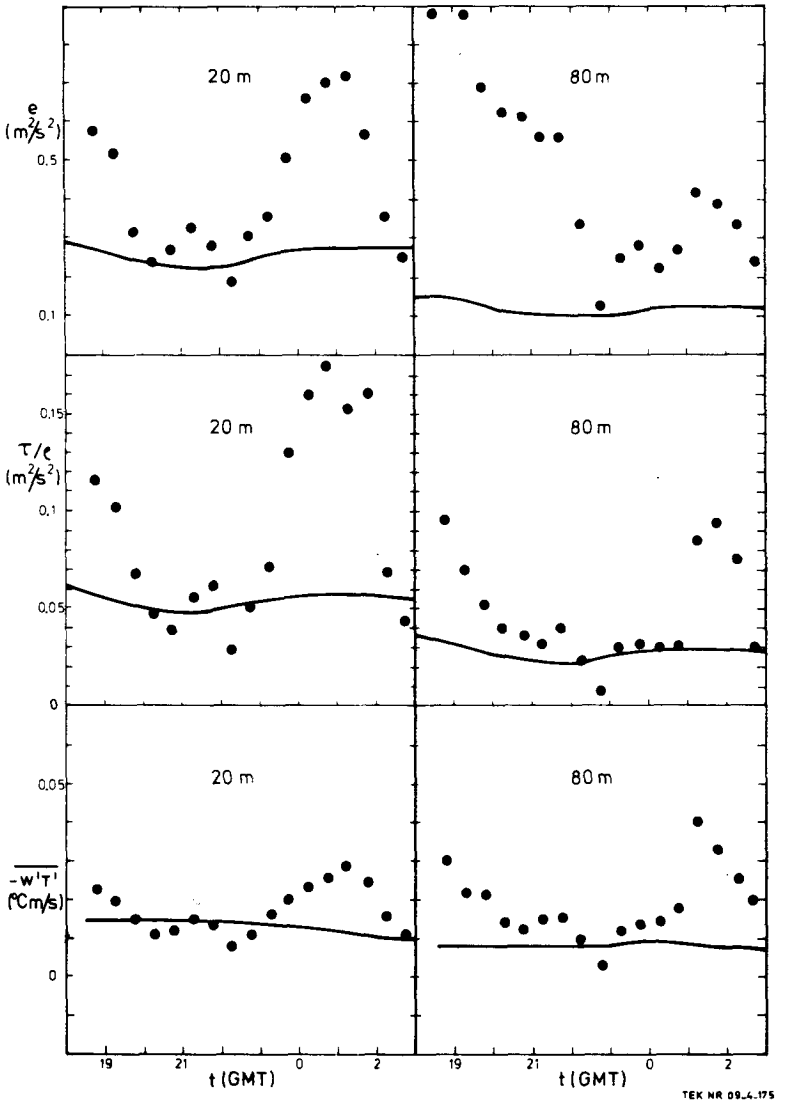

FIG. 6. Measured and calculated turbulent fluxes as a function of time for two observation heights: (solid line) calculations; (circles) observations.

match the measurements indicating that a stationary neutral condition is not a suitable starting condition in this case. The initial conditions are very important for the solution of (8) at heights where during the night turbulent fluxes vanish (in this case 200 m). There the solution of the model equations is dominated by an inertial oscillation. The phase and amplitude of this oscillation follow directly from the difference between the initial wind vector and the geostrophic wind (Blackadar, 1957).

We have calculated such an inertial oscillation for the wind vector at 200 m starting from the measured value at 1600 GMT (around sunset) and using a constant geostrophic wind of 10 m s^{-1} from 125°. The results are a wind maximum of 13.5 m s^{-1} at about 2200 GMT and a wind speed equal to the geostrophic wind at about 0130 GMT. The data of Fig. 4 show that this inertial oscillation describes the measured wind speeds at 200 m reasonably well.

The model calculations at 200 m also show an oscillation. This can be considered an inertial oscillation from the time that the calculated fluxes at 200 m are negligible (approximately 1800 GMT). Due to the initial conditions the agreement of calculated results with measurements in the first part of the night is poor.

The wind speeds at 20 and 80 m are on the average well simulated by the model. However, the measurements show an oscillation with a period of ~7 h, which is much smaller than the period $2\pi/f$ of an inertial oscillation. From Fig. 3 it follows that this oscillation also occurs simultaneously in the tem-

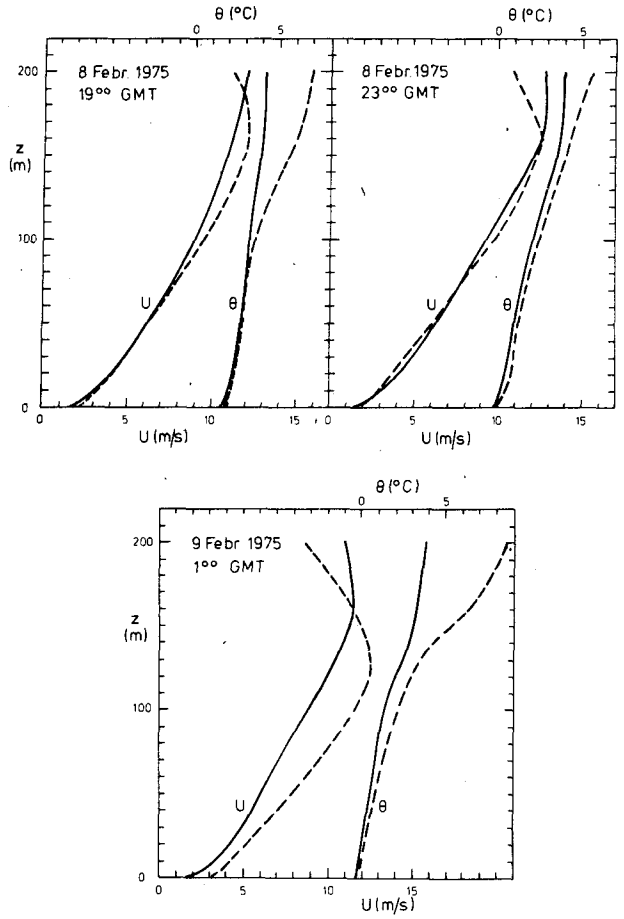

FIG. 7. Vertical profiles of measured and calculated wind speed and potential temperature: (solid line) calculation; (dashed line) observations.

perature at 200 m. The calculated results do not show these oscillations, because our model does not contain any processes with a time scale of 7 h. We have found similar oscillations in the observations during another night period.

The wind direction α as a function of time is shown in Fig. 5. An inertial oscillation would lead to a veering wind direction in the first part of the night and a wind direction equal to the geostrophic direction when the maximum wind speed is reached. This is approximately true for the calculated results at 200 m. However, the measured wind direction at this height veers with respect to the calculations at a rate of 2° h^{-1} until 2200 GMT and then remains approximately constant. Therefore, the veering in the measured wind direction cannot altogether be attributed to an inertial oscillation. At 80 m the measured direction also veers at a rate of 2° h^{-1} with respect to the calculated result, which is almost constant. These differences must be attributed to the neglected advection terms. From synoptic surface data we estimate that the horizontal temperature gradient inside the nocturnal boundary layer is of the order of 3×10^{-5} °C m^{-1} in a southeasterly direction. A thermal wind can then be calculated from (4). Since the observed wind is also in a southeasterly direction, the thermal wind will be perpendicular to the observed wind vector. The influence of the thermal wind will result in a change of wind direction. Using (2) this change can be approximated at a height z as $f\,|\mathbf{u}_{th}(z)|/|\mathbf{u}_H(z)|$. For 80 m this leads to a value of ~2° h^{-1} for the wind direction change in accordance with the observed results. At 200 m we find ~4° h^{-1}, which is somewhat larger than the veering of the observed wind direction with respect to the calculation. Therefore, we conclude that the difference between the measured and calculated wind direction can be attributed in this case principally to temperature advection.

At 10 m the measured and calculated wind directions are in good agreement in the first part of the night. The veering in the observed values after 2200 GMT is probably related to the veering at higher levels.

The measured and calculated turbulent fluxes are shown in Fig. 6. The fluxes at 200 m are not shown because they are negligible for most of the night. High levels of turbulence not found in the calculated results are present in the measurements. They occur simultaneously with oscillations in the wind speed and temperature, which were discussed in connection with Fig. 4. Because of the large time scale of this burst of turbulence (~3 h), we do not believe that it is caused by breaking gravity waves, which are known to produce intermittent high levels of turbulence in a stable boundary layer (Sethu-Raman, 1977). These high observed values of turbulence are responsible for the poor agreement between (20) and the observed boundary-layer height (Fig. 2).

As the time histories shown in Figs. 3, 4 and 5 give a poor impression of the vertical profiles, we show in Fig. 7 some characteristic profiles of the wind speed and the temperature. They indicate that the overall features of the observed profiles are reasonably well simulated by the model results.

7. Conclusions

Data obtained during a case study are compared with the results of a one-dimensional boundary-layer model. In this model turbulent fluxes are parameterized with the help of exchange coefficients. This parameterization is found to be consistent with the measurements.

The height of the turbulent nocturnal boundary layer grows to a stationary value of ~200 m. This height is reasonably well simulated by our model.

Above the boundary layer the flow is dominated by an inertial oscillation both in the observations

and in the calculations. Differences between the observed and calculated results at this height could be explained in our case in terms of temperature advection.

Inside the boundary layer, turbulent fluxes must be taken into account. The observations are reasonably well simulated by our model. Differences between model results and measurements are caused by advection. They increase with height.

Advection can have a considerable influence on the evolution of the nocturnal boundary layer. Its contribution was estimated in our observed results. However, we conclude that a one-dimensional boundary-layer model in which advection is neglected, can reasonably well simulate the boundary-layer height and the profiles of wind and temperature inside the nocturnal boundary layer.

Acknowledgment. The authors want to thank the Instrumental Division of their Institute for technical support, Messrs. J. G. van der Vliet and P. A. T. Nieuwendijk for their data management, and Mr. C. A. Engeldal for his assistance with the model calculations. They thank Dr. W. H. Kohsiek for the radiation calculations.

REFERENCES

Barr, S., and C. W. Kreitzberg, 1975: Horizontal variability and boundary layer modeling. *Bound.-Layer Meteor.*, **8**, 163–172.

Blackadar, A. K., 1957: Boundary layer wind maxima and their significance for the growth of nocturnal inversions. *Bull. Amer. Meteor. Soc.*, **38**, 283–290.

——, 1976: Modeling the nocturnal boundary layer. *Preprints 3rd Symposium Atmospheric Turbulence, Diffusion and Air Quality*, Raleigh, Amer. Meteor. Soc., 46–49.

Bodin, S. V., 1976: An unsteady one-dimensional atmospheric boundary layer model. Paper presented at the WMO Symposium on the Interpretation of Numerical Weather Prediction Products, Warsaw, 11–16 October.

Brost, R. A., and J. C. Wyngaard, 1978: A model study of the stably stratified planetary boundary layer. *J. Atmos. Sci.*, **35**, 1427–1440.

Busch, N. E., 1973: On the mechanics of atmospheric turbulence. *Workshop on Micrometeorology*, D. A. Haugen, Ed., Amer. Meteor. Soc., 1–66.

Businger, J. A., and S. P. S. Arya, 1974: Height of the mixed layer in the stably stratified planetary boundary layer. *Advances in Geophysics*, Vol. 18A, Academic Press, 73–92.

——, J. C. Wyngaard, Y. Izumi and E. F. Bradley, 1971: Flux-profile relationships in the atmospheric surface layer. *J. Atmos. Sci.*, **28**, 181–189.

Cats, G. J., 1977: The calculation of the geostrophic wind. Sci. Rep. 77-2, Royal Netherlands Meteorological Institute.

Delage, Y., 1974: A numerical study of the nocturnal atmospheric boundary layer. *Quart. J. Roy. Meteor. Soc.*, **100**, 351–364.

Djolov, G. D., 1974: Modeling of interdependent diurnal variation of meteorological elements in the boundary layer. *Chidrolog. Meteor. Sofia.*, **13**, 3–19.

Driedonks, A. G. M., H. van Dop and W. H. Kohsiek, 1978: Meteorological observations on the 213 m mast at Cabauw in the Netherlands. *Preprints 4th Symp. Meteorological Observations and Instrumentation*, Denver, Amer. Meteor. Soc., 41–46.

Elzasser, W. M., and M. F. Culbertson, 1960: *Atmospheric Radiation Tables. Meteor. Monogr.*, No. 23, 43 pp.

Frisch, A. S., and S. F. Clifford, 1974: A study of convection capped by a stable layer using Doppler Radar and acoustic echo sounders. *J. Atmos. Sci.*, **31**, 1622–1628.

Haltiner, G. J., 1971: *Numerical Weather Prediction.* Wiley, 317 pp.

Keller, H. B., 1971: A new difference scheme for parabolic problems. *Numerical Solution of Partial Differential Equations*, Vol. 3, Academic Press, 327–350.

SethuRaman, S., 1977: The observed generation and breaking of atmospheric gravity waves over ocean. *Bound.-Layer Meteor.*, **12**, 331–349.

Thorpe, A. J., and T. H. Guymer, 1977: The nocturnal jet. *Quart. J. Roy. Meteor. Soc.*, **103**, 633–653.

van Ulden, A. P., J. G. van der Vliet and J. Wieringa, 1976: Temperature and wind observations at heights from 2 to 200 m at Cabauw 1973. Sci. Rep. 76-7, Royal Netherlands Meteorological Institute, 17 pp.

Wieringa, J., 1967: Evaluation and design of wind vanes. *J. Appl. Meteor.*, **6**, 1114–1122.

Yu, T. W., 1977: A comparative study on parameterization of vertical turbulent exchange processes. *Mon. Wea. Rev.*, **105**, 57–66.

——, 1978: Determining height of the nocturnal boundary layer. *J. Appl. Meteor.*, **17**, 28–33.

Zilitinkevich, S. S., 1975: Resistance laws and prediction equations for the depth of the planetary boundary layer. *J. Atmos. Sci.*, **32**, 741–752.